SIFT: Modeling Solar-Induced Chlorophyll Fluorescence Over Sloping Terrain

Hanyu Shi, *Student Member, IEEE*, and Zhiqiang Xiao, *Member, IEEE*

***Abstract*— Solar-induced chlorophyll fluorescence (SIF) is found well correlated with gross primary productivity (GPP) and a good indicator of vegetation status. However, the influence of topography on SIF has not been studied, and SIF models with topographic consideration are needed to analyze this influence. Unfortunately, apart from computationally expensive 3-D models, current SIF models cannot work with sloping terrain. An efficient 1-D SIF model with topographic consideration (SIFT) is proposed in this study based on the well-known Soil Canopy Observation, Photochemistry and Energy fluxes (SCOPE) model. The evaluation of SIFT, by comparing with the 3-D Discrete Anisotropic Radiative Transfer (DART) model, demonstrates that it has high accuracy. This study also demonstrates that ignoring topography induces significant errors (exceeding 125% for a 60° slope) in canopy SIF simulations. The conclusion that the topography is an important factor for SIF and the proposed SIFT model will benefit those who are interested in SIF simulations and applications.**

***Index Terms*— Solar-induced chlorophyll fluorescence (SIF), SIF model with topographic consideration (SIFT), Soil Canopy Observation, Photochemistry and Energy fluxes (SCOPE), topography.**

I. Introduction

SOLAR-INDUCED chlorophyll fluorescence (SIF) is a good indicator of vegetation status. SIF is emitted by photosynthetic machinery during photosynthesis, and its emission spectrum falls in the range of 640–850 nm. Recent studies have shown that SIF is well correlated with the gross primary productivity (GPP), which provides a bridge for global carbon studies through remote-sensing observations [1], [2]. At the canopy scale, SIF is observed after three processes: absorption of photosynthetically active radiation, emission of fluorescence by photosystem, and scattering and reabsorption of the emitted fluorescence [3]. Generally, the observed SIF at the canopy scale is influenced by physiological and nonphysiological factors, such as nonphotochemical quenching, temperature, light intensity, and leaf angle distribution (LAD). These factors have been modeled in certain physiological and radiative transfer models of leaves and canopy for fluorescence (see [4] for review of the models). Among these models, the 1-D Soil Canopy Observation, Photochemistry and Energy fluxes (SCOPE) model [5] has delivered successful results. SCOPE is an integration of the radiative transfer and energy balance model, which has been widely used for SIF studies [4]. Even though these SIF models have been employed in several applications, none of them, to the best of our knowledge, has been able to incorporate topographic effects in canopy SIF simulations, except 3-D radiative transfer models. Although 3-D radiative transfer models can model topographic surfaces, they are computationally expensive and require huge memory space that limits their applicability.

The topography changes the solar-target-sensor geometries, affects radiation fields, and alters the observed radiance by sensors [6]. As part of the observed radiance at the canopy scale, SIF is anisotropic and affected by the topography. Although the topographic effects on certain surface parameters (e.g., shortwave and longwave radiation, albedo, and surface reflectance) have been studied, and the related models were developed [7]–[16], the influences of topography on SIF have not been analyzed to date. Considering the significance of SIF in ecological studies and the fact that rugged terrains occupy about 24% of the global land surface [17], developing an efficient SIF model with topographic consideration (SIFT) and analyzing topographic effects on SIF are essential for the development of SIF studies.

We develop a 1-D SIFT based on the SCOPE-SIF model. The proposed model considers the influences of topography on: 1) the direct solar radiation and the obstruction of the surrounding topography for diffuse solar radiation and 2) the gravitropic influences on LAD. The proposed SIFT is evaluated by the 3-D Discrete Anisotropic Radiative Transfer (DART) ray-tracing model. DART has been recognized as a benchmark for radiative transfer model in the optical remote sensing field [18], [19] and proven to be accurate over rugged areas [20].

II. Methodology

A. Model

The SCOPE-SIF model is designed for flat surfaces, and the canopy is horizontally placed, as shown in Fig. 1(a). The directional SIF at the top-of-canopy (TOC) is expressed as [5], [21]

$$L_F = L_s + L_d + L_c. \tag{1}$$

L_s and L_d are the fluorescence of the sunlit and shaded leaves in the viewing direction, respectively, and L_c is the

Manuscript received September 12, 2020; revised November 20, 2020 and January 8, 2021; accepted March 17, 2021. This work was supported by the National Natural Science Foundation of China under Grant 41771359. *(Corresponding author: Zhiqiang Xiao.)*

The authors are with the State Key Laboratory of Remote Sensing Science, Faculty of Geographical Science, Beijing Normal University, Beijing 100875, China (e-mail: shihanyu@mail.bnu.edu.cn; zhqxiao@bnu.edu.cn).

Color versions of one or more figures in this letter are available at https://doi.org/10.1109/LGRS.2021.3067879.

Digital Object Identifier 10.1109/LGRS.2021.3067879

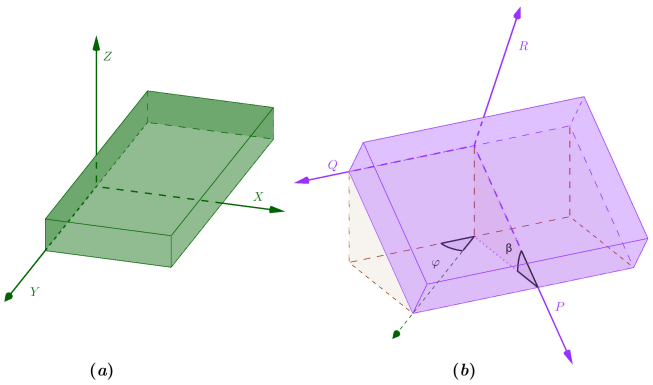

Fig. 1. Coordinates for (a) horizontal surface (XYZ), i.e., the SCOPE model, and (b) sloping surface (PQR), i.e., the SIFT model. The slope and aspect values are β and φ, respectively. The green cuboid represents a canopy layer that lays on the flat surface, while the purple cuboid indicates that the canopy layer is put on a sloping surface.

fluorescence that is scatted by the leaves and soil. The three parts are calculated by (2), shown at the bottom of the page, where the optical depth of the canopy layer (x) starts from -1 (bottom of canopy) to 0 (top of canopy). LAI(x) is the leaf area index (LAI) refers to the soil surface at x, Ω_l indicates the direction of leaf normal, and Ω_s and Ω_o are the solar and view directions. λ_e is the excitation wavelength ranging from 400 to 750 nm, and λ_f is the emission wavelength ranges from 640 to 850 nm. E_s, E^+, and E^- are the direct solar irradiance, upward diffuse irradiance, and downward diffuse irradiance in the canopy, respectively. P_o is the probability that a sublayer is observed, and P_{so} is the bidirectional gap fraction. The terms F^- and F^+ are the downward and upward fluorescences, respectively, and r_s is the soil reflectance. υ and υ' are scattering coefficients for downward and upward diffuse radiations into view direction, respectively; υ_F, υ'_F, and w_F are fluorescence emission coefficients. ϕ'_{fs} and ϕ'_{fd} are fluorescence amplification factors for sunlit and shaded leaves, respectively. $g(\Omega_l)$ is the leaf area orientation density function [some literature use $g(\Omega_l)/(2\pi)$], which satisfies

$$\int_0^{\pi/2}\int_0^{2\pi} g(\Omega_l)d\Omega_l = 1. \tag{3}$$

In the SCOPE model that suits flat surfaces, the leaves are assumed uniformly distributed over the azimuth, and the leaf inclination density function (LIDF) $f(\theta_l)$ is used to replace $g(\Omega_l)$

$$f(\theta_l) = 2\pi\, g(\Omega_l)\sin\theta_l \tag{4}$$

where θ_l is the leaf inclination angle.

Particularly, E^+, E^-, F^-, and F^+ in (2) are calculated from incident solar radiation at TOC (i.e., E_{sun} and E_{sky}). The details of the calculation can be found in [5]. The incident direct solar radiation (E_{sun}) and diffuse solar radiation (E_{sky}) at TOC are mentioned here because they are served as input, and topography changes them directly.

The PQR coordinate system is built on the sloping surface (with a slope of β and aspect of φ) for the proposed SIFT model over sloping terrain, as shown in Fig. 1(b). The purple cuboid represents a canopy on a slope. In contrast, the green cuboid is a horizontally placed canopy in Fig. 1(a). The normal to the horizontal canopy is $\boldsymbol{n} = (0; 0; 1)$, and the normal to the sloping canopy is $\boldsymbol{t} = (\sin\beta\cos\varphi; \sin\beta\sin\varphi; \cos\beta)$ in the XYZ coordinate system. A direction can be expressed by using a vector $\boldsymbol{p}^h = (\sin\theta_p^h\cos\varphi_p^h; \sin\theta_p^h\sin\varphi_p^h; \cos\theta_p^h)$ in the XYZ coordinate and $\boldsymbol{p}^t = (\sin\theta_p^t\cos\varphi_p^t; \sin\theta_p^t\sin\varphi_p^t; \cos\theta_p^t)$ in the PQR coordinate (the superscripts "h" and "t" indicate that variables are referred to the XYZ and PQR coordinate systems, respectively). The transformation between $\boldsymbol{p}^h$ and $\boldsymbol{p}^t$ is

$$\boldsymbol{p}^t = R_y(\beta)R_z(\varphi)\boldsymbol{p}^h \tag{5}$$

where R_z and R_y are the rotation matrices

$$R_z = \begin{bmatrix} \cos\varphi & \sin\varphi & 0 \\ -\sin\varphi & \cos\varphi & 0 \\ 0 & 0 & 1 \end{bmatrix}, \quad R_y = \begin{bmatrix} \cos\beta & 0 & -\sin\beta \\ 0 & 1 & 0 \\ \sin\beta & 0 & \cos\beta \end{bmatrix}. \tag{6}$$

The relationship between incident radiation on a sloping surface and on a horizontal plane is given as follows [6], [22]:

$$E_{\text{sun}}(\Omega_s^t) = F_{\text{sun}}E_{\text{sun}}(\Omega_s^h) \tag{7a}$$
$$E_{\text{sky}}(\Omega_{2\pi}^t) = F_{\text{sky}}E_{\text{sky}}(\Omega_{2\pi}^h) \tag{7b}$$
$$F_{\text{sun}} = \zeta\cos\theta_s^t/\cos\theta_s^h \tag{7c}$$
$$F_{\text{sky}} = k\cos\theta_s^t/\cos\theta_s^h + (1-k)V_{\text{sky}} \tag{7d}$$

where F_{sun} and F_{sky} are the terrain factors for the direct and diffuse radiations, respectively; ζ is a binary factor (0 or 1) that indicates whether the pixel is self-shadowed or shielded by other pixels [6], [23], [24]; θ_s^h and θ_s^t are solar zenith angles

$$L_s(\lambda_f) = \frac{1}{\pi}\int_{-1}^{0}\text{LAI}(x)P_{\text{so}}(x,\Omega_s,\Omega_o)\int_0^{2\pi}\int_0^{\pi/2}\phi'_{fs}(x,\Omega_l)\int_{400}^{750}\big[w_F(\lambda_f,\lambda_e,\Omega_l)E_s(\lambda_e,\Omega_s) + \upsilon_F(\lambda_f,\lambda_e,\Omega_l)E^-(\lambda_e,x,\Omega_{2\pi}) + \upsilon'_F(\lambda_f,\lambda_e,\Omega_l)E^+(\lambda_e,x,\Omega_{2\pi})\big]g(\Omega_l)d\lambda_e d\Omega_l dx \tag{2a}$$

$$L_d(\lambda_f) = \frac{1}{\pi}\int_{-1}^{0}\text{LAI}(x)(P_o(x,\Omega_o) - P_{\text{so}}(x,\Omega_s,\Omega_o))\phi'_{fd}(x)\int_0^{2\pi}\int_0^{\pi/2}\int_{400}^{750}\big[\upsilon_F(\lambda_f,\lambda_e,\Omega_l)E^-(\lambda_e,x,\Omega_{2\pi}) + \upsilon'_F(\lambda_f,\lambda_e,\Omega_l)E^+(\lambda_e,x,\Omega_{2\pi})\big]g(\Omega_l)d\lambda_e d\Omega_l dx \tag{2b}$$

$$L_c(\lambda_f) = \frac{1}{\pi}\int_{-1}^{0}\text{LAI}(x)P_o(x,\Omega_o)\int_0^{2\pi}\int_0^{\pi/2}\big[\upsilon(\Omega_l)F^-(\lambda_f,x) + \upsilon'(\Omega_l)F^+(\lambda_f,x)\big]g(\Omega_l)d\lambda_e d\Omega_l dx + \frac{1}{\pi}P_o(-1,\Omega_o)r_s(\lambda_f)F^-(\lambda_f,-1) \tag{2c}$$

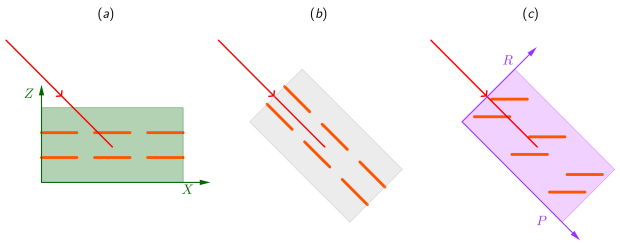

Fig. 2. Illustration of the topographic and gravitropic effects on LAD. Red lines with an arrow are sun rays; solid orange lines represent leaves. (a) LAD over a flat surface [assume leaves are parallel to the horizontal plane (i.e., $\theta_l = 0$)]. LAD over a sloping surface: (b) without considering gravitropism and (c) with gravitropism considered.

that are relative to the horizontal and sloping canopies, respectively; and F_{sky} considers both the isotropic and anisotropic circumsolar diffuse irradiance, whereas k is the proportion of anisotropic components to total diffuse irradiance [25]. Practically, k can be approximated by the direct transmittance of the atmosphere [6], [25], but the isotropic diffuse radiation assumption was adopted in this study. Thus, $F_{\text{sky}} = V_{\text{sky}}$, where V_{sky} is the sky view factor, defined as the relative proportion of the visible sky.

Essentially, the topographic algorithm rotates the canopy layer and makes it parallel to the sloping surface. Except for the radiation intercepted by the canopy, LAI is also changed to keep leaf areas identical since different reference planes are used, which is

$$\text{LAI}^t = \text{LAI}^h \cos\beta \tag{8}$$

where LAI^h is the LAI referred to a flat area (XY plane) and LAI^t is the LAI referred to a sloping area (PQ plane). Another changed variable is LAD, as shown in Fig. 2. The leaves cannot be simply rotated owing to the gravitropism of plants. As shown in Fig. 2(c), LAD has been changed in the sloping coordinate (PQR), and the leaf angles in PQR are modeled by

$$\boldsymbol{l}^t = R_y(\beta)R_z(\varphi)\boldsymbol{l}^h \tag{9}$$

where $\boldsymbol{l}^h = (\sin\theta_l^h\cos\varphi_l^h;\ \sin\theta_l^h\sin\varphi_l^h;\ \cos\theta_l^h)$ and $\boldsymbol{l}^t = (\sin\theta_l^t\cos\varphi_l^t;\ \sin\theta_l^t\sin\varphi_l^t;\ \cos\theta_l^t)$ are the upward normals to the leaf in the XYZ and PQR coordinates, respectively. Fig. 2 also demonstrates that the assumption of leaf-azimuth-independence in SCOPE is not valid in the PQR coordinate. Therefore, LIDF, as given in (4), does not work over the sloping terrain, and hence, the influences of leaf azimuth angles should be considered [see (2)].

To summarize, $E_{\text{sun}}(\Omega_s^h)$, $E_{\text{sky}}(\Omega_{2\pi}^h)$, LAI^h, and $g(\Omega_l^h)$ [or $f(\theta_l^h)$] are input to (2) for calculating canopy fluorescence (L_F) in SCOPE-SIF. In the proposed SIFT model, $E_{\text{sun}}(\Omega_s^t)$, $E_{\text{sky}}(\Omega_{2\pi}^t)$, LAI^t, and $g(\Omega_l^t)$ are first calculated through (5) and (9) and are then input to (2) to calculate L_F over sloping terrain.

B. Evaluation

The proposed SIFT model was evaluated by comparing it with the well-known 3-D DART model. The BOA irradiance spectra (400–850 nm) were presimulated according to the atmospheric conditions and solar positions using the MODerate resolution atmospheric TRANsmission (MODTRAN) model and are input into the DART and SIFT to simulate the canopy SIF. The parameter settings for the model comparison are listed in Table I. Three atmospheric conditions were predefined, namely, a molecular atmosphere, an aerosol atmosphere with an aerosol optical depth (AOD) of 0.2, and a cloudy atmosphere with a cloud optical depth of 8.0. The 1976 U.S. standard atmosphere, the rural aerosol type, and the default standard cirrus model were used, respectively. A gentle slope (10°) and a steep slope (40°) were used for terrain conditions. The solar and view zenith angles relative to the horizontal plane ranged from 0° to 40°, and thus, the corresponding zenith angle relative to the slope spans from 0° to 80°. Two LAI values and six typical LAD functions were simulated. The simulations were conducted at a 10-nm interval between 400 and 850 nm. Without loss of generality, the biochemical variables and fluorescence quantum yield efficiency are fixed to the DART default values, the fluorescence amplification factors are set to 1, and the hotspot factor is not used. For convenience, the approximation method proposed by Liu and Jordan [26] was employed in this study to calculate V_{sky}. More accurate methods may be adopted in practical applications with the help of the digital elevation model (DEM) data [23], [24], [27].

TABLE I

PARAMETER SETTINGS FOR COMPARING DART AND THE PROPOSED SIF MODEL (LAD = LEAF ANGLE DISTRIBUTION)

Parameter	Values	Units
For MODTRAN	molecular atmosphere aerosol atmosphere cloud atmosphere	-
Solar zenith angle	5, 15, 25, 35	degrees
Solar azimuth angle	0	degrees
View zenith angle	0, 10, 20, 30, 40	degrees
View azimuth angle	0, 90, 180, 270	degrees
Slope	10, 40	degrees
Aspect	0, 90, 180	degrees
Leaf area index	2, 6	m^2/m^2
LAD	uniform, plagiophile, erectophile, planophile, extremophile, spheric	-

III. RESULTS AND ANALYSES

A. Model Evaluation

The proposed SIFT model was evaluated by comparing it with DART, and the results from the SCOPE-SIF model were also compared with DART.

The comparison of the scatter of canopy fluorescence between SIFT and DART is shown in Fig. 3(a). It is observed that the SIFT model satisfactorily agree with the DART model, with a root mean square error (RMSE) value of 0.05 $\text{W/m}^2/\mu\text{m/sr}$, a mean bias error (MBE) value of 0.007 $\text{W/m}^2/\mu\text{m/sr}$, and the coefficient of determination $R^2 > 0.99$. The result of comparison for the SCOPE-SIF

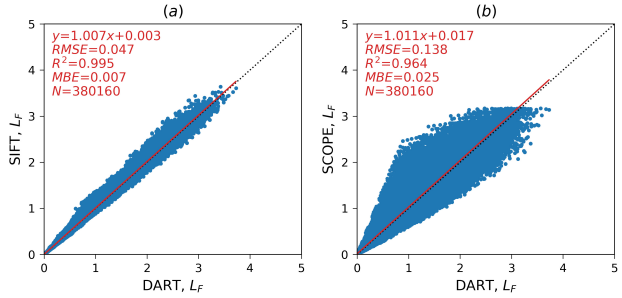

Fig. 3. Evaluation of the canopy fluorescence (in W/m^2/μm/sr) simulated by (a) proposed SIFT model and (b) SCOPE-SIF model.

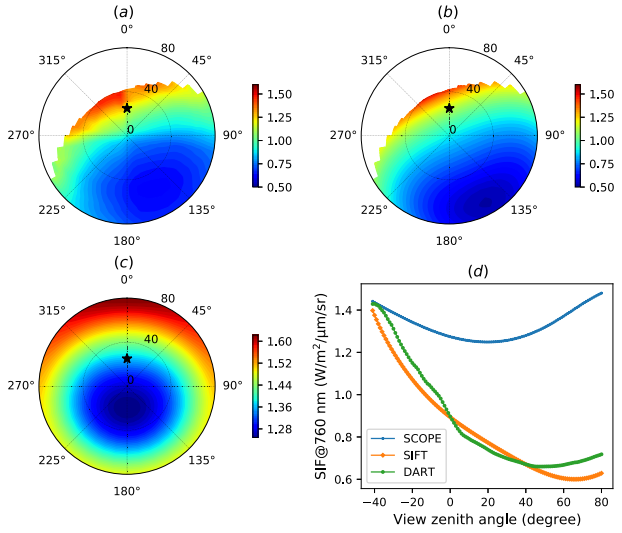

Fig. 4. Comparisons of canopy fluorescence (W/m^2/μm/sr) at 760 nm simulated over 2π space by (a) DART, (b) SIFT, and (c) SCOPE models. (d) Comparison of the three models at the solar plane. The black stars indicate sun positions. (Spheric LAD; solar zenith angle 25°; solar azimuth angle 0°; slope 45°; and aspect 150°.)

model is shown in Fig. 3(b), and significant differences have been observed, which demonstrates that ignoring topographic effects induce errors for SIF simulations.

An example for a hemispherical distribution of canopy fluorescence is shown in Fig. 4, where SIF at 760 nm is plotted. The BOA irradiance corresponds to the aerosol atmosphere defined in Table I for a solar zenith angle of 25°. The slope and aspect are 45° and 150°, respectively, and the spheric LAD has been used. The no-data regions in Fig. 4(a) and (b) indicate that the canopy is not visible by the sensor. As shown in Fig. 4(a) and (b), SIFT has the same patterns as DART. However, the SCOPE-SIF model, as shown in Fig. 4(c), does not capture the influences of topography. The comparison of SIF values at the solar plane is shown in Fig. 4(d). Although minuscule differences in the SIF values have been found between SIFT and DART, they display the same change patterns. In contrast, SCOPE-SIF does not reflect the influences of topography, and it has large discrepancies with respect to DART over sloping terrain.

B. Influences of Topography

The errors induced by ignoring the topographic effects have been analyzed for different slopes using the SCOPE-SIF and

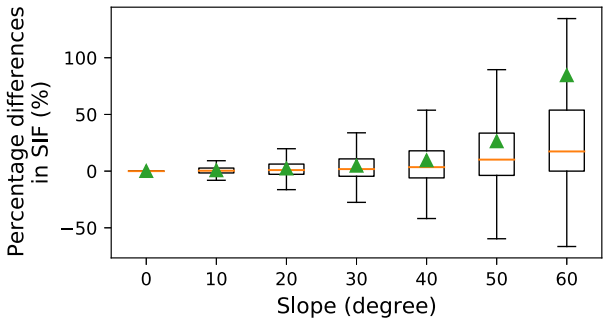

Fig. 5. Percentage differences in canopy fluorescence (W/m^2/μm/sr) simulated by the SCOPE-SIF and SIFT models with increasing terrain slope. The orange lines indicate median values, and the green triangles indicate mean values.

SIFT models. The parameter configurations are expanded from Table I, with slope values ranging from 0° to 60° at 10° intervals; besides, the SIF within 640–850 nm have all been analyzed. The percentage differences in the simulated SIF by the SCOPE-SIF and SIFT models for increasing terrain slope (calculated as (SCOPE-SIF − SIFT)/SIFT × 100%) are shown as boxplots in Fig. 5. It shows that the difference in the canopy SIF increases with the slope angle and exceeds 125% for a 60° slope. Fig. 5 demonstrates that ignoring the topographic effects can introduce significant errors in the canopy SIF.

IV. Discussion

Evaluation results demonstrate that the proposed SIFT model is accurate, but several issues need to be discussed to improve it in the future.

The first issue is the contribution from adjacent slopes [22]. Radiation from surrounding slopes is another source of incoming radiation to the target slope. This contribution is usually insignificant and can be neglected, but it is important for highly reflective surfaces or deep valleys areas [6]. The adjacent contributions are not modeled in this study because it is small for vegetated areas, especially at the visible spectrum range absorbed by vegetation to emit fluorescence. Nevertheless, adjacent contributions for SIF simulation can be accurately modeled using the algorithm proposed in [22]. The next version of SIFT by introducing this algorithm is being tested and will be released in the future.

The second issue is composite-slope modeling [10]. A pixel (e.g., 1 km) contains many solo slopes unless the spatial resolution is very high. Composite-slope modeling is important when applying surface models to remote sensing data [9], [10], [14]. The SIFT model proposed in this study is for solo slopes, and composite-slope modeling for SIF is under development and will be present in a subsequent study.

The third issue is the heterogeneous canopy. SIFT is based on the SCOPE-SIF model, and thus, it is only suitable for homogeneous canopy. A potential improvement of SIFT is to combine it with geometric optical models for heterogeneous canopies [13].

V. Conclusion

Neglecting topographic effects on SIF induces significant errors is demonstrated in this study, and the error can be

large than 125% for a 60° slope. The error in SIF may be introduced in further studies, such as GPP estimations, and thus, it causes unnecessary uncertainties. This study proposed an SIFT model to eliminate the error induced by topography. By adding only three variables (slope, aspect, and F_{sky}) to the SCOPE-SIF model, the proposed SIFT model can simulate canopy fluorescence over sloping terrain. The evaluation of the proposed SIFT model in comparison with DART demonstrated its high accuracy. Besides, SIFT efficiently models radiative transfer processes, and it is much faster than DART because DART needs to trace lots of rays in many voxels to get accurate results.

The proposed model and the finding that topography is an essential factor for fluorescence can benefit researchers interested in SIF, GPP, and other related studies. For example, it may be used to develop simplification factors [28] for SIF correction over sloping terrain, it can improve the estimation of escape probability [29] and normalize directional effects of SIF [30] over sloping terrain, and it may compensate for the uncertainties in the SIF–GPP relationship [1].

ACKNOWLEDGMENT

The authors would like to thank Dr. Christiaan van de Tor for sharing the SCOPE code on GitHub and Dr. Jean-Philippe Gastellu-Etchegorry for providing the DART software. They also thank the anonymous reviewers for providing helpful comments and suggestions.

REFERENCES

[1] Y. Ryu, J. A. Berry, and D. D. Baldocchi, "What is global photosynthesis? History, uncertainties and opportunities," *Remote Sens. Environ.*, vol. 223, pp. 95–114, Mar. 2019.

[2] X. Wang, J. M. Chen, and W. Ju, "Photochemical reflectance index (PRI) can be used to improve the relationship between gross primary productivity (GPP) and sun-induced chlorophyll fluorescence (SIF)," *Remote Sens. Environ.*, vol. 246, Sep. 2020, Art. no. 111888.

[3] P. Yang *et al.*, "Using reflectance to explain vegetation biochemical and structural effects on sun-induced chlorophyll fluorescence," *Remote Sens. Environ.*, vol. 231, Sep. 2019, Art. no. 110996.

[4] G. H. Mohammed *et al.*, "Remote sensing of solar-induced chlorophyll fluorescence (SIF) in vegetation: 50 years of progress," *Remote Sens. Environ.*, vol. 231, Sep. 2019, Art. no. 111177.

[5] C. van der Tol, W. Verhoef, J. Timmermans, A. Verhoef, and Z. Su, "An integrated model of soil-canopy spectral radiances, photosynthesis, fluorescence, temperature and energy balance," *Biogeosciences*, vol. 6, no. 12, pp. 3109–3129, Dec. 2009.

[6] A. Mousivand, W. Verhoef, M. Menenti, and B. Gorte, "Modeling top of atmosphere radiance over heterogeneous non-Lambertian rugged terrain," *Remote Sens.*, vol. 7, no. 6, pp. 8019–8044, Jun. 2015.

[7] G. Yin, A. Li, W. Zhao, H. Jin, J. Bian, and S. Wu, "Modeling canopy reflectance over sloping terrain based on path length correction," *IEEE Trans. Geosci. Remote Sens.*, vol. 55, no. 8, pp. 4597–4609, Aug. 2017.

[8] J. Geng *et al.*, "GOFP: A geometric-optical model for forest plantations," *IEEE Trans. Geosci. Remote Sens.*, vol. 55, no. 9, pp. 5230–5241, Sep. 2017.

[9] D. Hao *et al.*, "Modeling anisotropic reflectance over composite sloping terrain," *IEEE Trans. Geosci. Remote Sens.*, vol. 56, no. 7, pp. 3903–3923, Jul. 2018.

[10] J. Wen *et al.*, "Characterizing land surface anisotropic reflectance over rugged terrain: A review of concepts and recent developments," *Remote Sens.*, vol. 10, no. 3, p. 370, Feb. 2018.

[11] S. Wu, J. Wen, D. You, H. Zhang, Q. Xiao, and Q. Liu, "Algorithms for calculating topographic parameters and their uncertainties in downward surface solar radiation (DSSR) estimation," *IEEE Geosci. Remote Sens. Lett.*, vol. 15, no. 8, pp. 1149–1153, Aug. 2018.

[12] S. Wu *et al.*, "Characterization of remote sensing albedo over sloped surfaces based on DART simulations and *in situ* observations," *J. Geophys. Res., Atmos.*, vol. 123, no. 16, pp. 8599–8622, Aug. 2018.

[13] S. Wu *et al.*, "Modeling discrete forest anisotropic reflectance over a sloped surface with an extended GOMS and SAIL model," *IEEE Trans. Geosci. Remote Sens.*, vol. 57, no. 2, pp. 944–957, Feb. 2019.

[14] D. Hao, J. Wen, Q. Xiao, D. You, and Y. Tang, "An improved topography-coupled kernel-driven model for land surface anisotropic reflectance," *IEEE Trans. Geosci. Remote Sens.*, vol. 58, no. 4, pp. 2833–2847, Apr. 2020.

[15] H. Shi and Z. Xiao, "The 4SAILT model: An improved 4SAIL canopy radiative transfer model for sloping terrain," *IEEE Trans. Geosci. Remote Sens.*, early access, Sep. 22, 2020, doi: 10.1109/TGRS.2020.3022874.

[16] G. Yan, Z.-H. Jiao, T. Wang, and X. Mu, "Modeling surface longwave radiation over high-relief terrain," *Remote Sens. Environ.*, vol. 237, Feb. 2020, Art. no. 111556.

[17] S. Wu *et al.*, "The definition of remotely sensed reflectance quantities suitable for rugged terrain," *Remote Sens. Environ.*, vol. 225, pp. 403–415, May 2019.

[18] E. Grau and J.-P. Gastellu-Etchegorry, "Radiative transfer modeling in the Earth—Atmosphere system with DART model," *Remote Sens. Environ.*, vol. 139, pp. 149–170, Dec. 2013.

[19] J.-P. Gastellu-Etchegorry *et al.*, "DART: Recent advances in remote sensing data modeling with atmosphere, polarization, and chlorophyll fluorescence," *IEEE J. Sel. Topics Appl. Earth Observ. Remote Sens.*, vol. 10, no. 6, pp. 2640–2649, Jun. 2017.

[20] Y. Wang, N. Lauret, and J.-P. Gastellu-Etchegorry, "DART radiative transfer modelling for sloping landscapes," *Remote Sens. Environ.*, vol. 247, Sep. 2020, Art. no. 111902.

[21] C. van der Tol, N. Vilfan, D. Dauwe, M. P. Cendrero-Mateo, and P. Yang, "The scattering and re-absorption of red and near-infrared chlorophyll fluorescence in the models fluspect and SCOPE," *Remote Sens. Environ.*, vol. 232, Oct. 2019, Art. no. 111292.

[22] C. Proy, D. Tanre, and P. Deschamps, "Evaluation of topographic effects in remotely sensed data," *Remote Sens. Environ.*, vol. 30, no. 1, pp. 21–32, Oct. 1989.

[23] J. Dozier, J. Bruno, and P. Downey, "A faster solution to the horizon problem," *Comput. Geosci.*, vol. 7, no. 2, pp. 145–151, Jan. 1981.

[24] J. Dozier and J. Frew, "Rapid calculation of terrain parameters for radiation modeling from digital elevation data," *IEEE Trans. Geosci. Remote Sens.*, vol. 28, no. 5, pp. 963–969, Sep. 1990.

[25] J. E. Hay, "Calculating solar radiation for inclined surfaces: Practical approaches," *Renew. Energy*, vol. 3, nos. 4–5, pp. 373–380, Jun. 1993.

[26] B. Y. H. Liu and R. C. Jordan, "The interrelationship and characteristic distribution of direct, diffuse and total solar radiation," *Sol. Energy*, vol. 4, no. 3, pp. 1–19, Jul. 1960.

[27] Z.-H. Jiao, H. Ren, X. Mu, J. Zhao, T. Wang, and J. Dong, "Evaluation of four sky view factor algorithms using digital surface and elevation model data," *Earth Space Sci.*, vol. 6, no. 2, pp. 222–237, Feb. 2019.

[28] G. Yin *et al.*, "PLC: A simple and semi-physical topographic correction method for vegetation canopies based on path length correction," *Remote Sens. Environ.*, vol. 215, pp. 184–198, Sep. 2018.

[29] C. Frankenberg and J. Berry, "Solar induced chlorophyll fluorescence: Origins, relation to photosynthesis and retrieval," in *Comprehensive Remote Sensing*, vol. 3, S. Liang, Ed. Oxford, U.K.: Elsevier, Jan. 2018, pp. 143–162.

[30] D. Hao *et al.*, "Practical approaches for normalizing directional solar-induced fluorescence to a standard viewing geometry," *Remote Sens. Environ.*, vol. 255, Mar. 2021, Art. no. 112171.